Project funded by the European Commission under the 6th (EC) RTD Framework Programme (2002- 2006) within the framework of the specific research and technological development programme “Integrating and strengthening the European Research Area”

Project UpWind

Contract No.:
019945 (SES6)

“Integrated Wind Turbine Design”

AUTHOR:	Boris Jasniewicz
AFFILIATION:	Fraunhofer IWES
ADDRESS:	Königstor 59, D-34119 Kassel
TEL.:	+49 561 7294287
EMAIL:	bjasniewicz@iwes.fraunhofer.de
FURTHER AUTHORS:	
REVIEWER:	Martin Geyler
APPROVER:	

Document Information

DOCUMENT TYPE	Deliverable 5.3
DOCUMENT NAME:	Online estimation of mechanical loads for wind turbines
REVISION:	
REV.DATE:	
CLASSIFICATION:	R0: General public
STATUS:	

Abstract: This work deals with the online estimation of mechanical loads for monitoring and control applications. Standard measurement signals are employed to estimate the tower bending moments using a state-space observer. Good estimation results are obtained with field test data from a commercially available 5MW turbine.

Contents

Status				Confidentiality				Accessibility	
S0	Approved/Released			**R0**	General public	X		Private web site	
S1	Reviewed			**R1**	Restricted to project members			Public web site	X
S2	Pending for review			**R2**	Restricted to European. Commission			Paper copy	
S3	Draft for commends			**R3**	Restricted to WP members + PL				
S4	Under preparation			**R4**	Restricted to Task members +WPL+PL				

PL: *Project leader* **WPL:** *Work package leader* **TL:** *Task leader*

1 Introduction

The size of wind turbines has constantly increased in the last three decades. This has lead to the application of more lightweight components, which, in turn, has resulted in more flexible structures. Thus, structural loads have become even more important. The issues related to structural load can be overcome by monitoring these loads and by mitigating them with appropriate control measures. For these purposes, the online estimation of loads is very useful.

One field of application is condition monitoring of extreme and fatigue loads, in terms of both maintenance and operating control. Although off-line data processing is sufficient for long term influences, the continuous estimation is useful if a rapid influence from the operating control to changing wind conditions is intended.

Another very important field of application is to provide a basis for feedback control measures to reduce mechanical loads. Estimated loads can be used as input signals for load reducing controllers instead of directly measured strain. This is beneficial in two respects. Sensor installation is not only costly due to installation and maintenance, but sensor faults themselves might lead to turbine malfunction – which implies yet another field of application.

Hence, this report, which continues the work reported in [5], focuses on tower and blade load estimation that is based on measurements available on today's large scale wind turbines.

Three different time scales can be established according to the application area:

- A slow time scale referring to the offline calculation of extreme and fatigue loads in terms of maintenance,
- a medium time scale if rapid response of the operating control to changing conditions is intended, and
- a fast time scale for load reducing feedback control measures.

The continuous estimation method based on state-space observers investigated in this report is suitable for all three time scales. A state-space observer uses a state-space model of the system or signal to be observed. It employs measurements of the system to continuously update the states of those models, which are running in parallel with the real processes.

Because the intended applications are in the field of control simple linear time-invariant models are used in this study. The main results are based on a linear time-invariant state-space model of the whole turbine for a distinct operating point [6]. It is described in detail in section 2.2. Its mechanical part is obtained from the linearization of a multibody model of the wind turbine's structure consisting of rigid beams, which are connected by spring/damper pairs. Thus, the main structural modes are represented.

The input of the model is the undisturbed, free wind speed, which can not be measured accurately enough by the usually installed anemometer on top of the nacelle. Therefore, the wind speed has to be estimated as well. Two methods for wind speed estimation are investigated, see section 2.3. The first one is called external estimation and uses measurements of the electrical power, the rotor speed and the collective pitch angle provided by the operating control system. The second method is called internal estimation and consists of a linear signal model, which is combined with the wind turbine model, and whose states are also estimated by the observer.

For updating the current states the observer employs four measurement signals: the readings of the accelerometers measuring the tower top longitudinal and lateral motion, the rotor speed measurement, and the pitch angle commanded by the collective pitch controller, each of which is a readily available signal on today's large scale wind turbines. The applied observer is a linear

quadratic estimator, the so-called Kalman-Bucy filter [1]. That is, uncertainties are modelled by Gaussian noise. An intuitive, easy to use design procedure is suggested. Observer related topics can be found in section 3.

Estimating wind speed and turbine states by state space observers has been proposed earlier [4] and is used in several studies, see for example [10],[11],[12] – even though many of them use those in the context of state-space controllers and do not explicitly account for the estimation performance.

Field test data that is obtained from a commercial 5MW wind turbine [7] is used for the validation of the approach, see section 4. To this end, strain gauges have been attached to the tower and the blades in addition to the four measurements signals used by the observer as mentioned above. Then, the measured and the estimated bending moments are compared. The results presented in section 4.2 show that the four measurement signals provide a sufficient basis for the estimation of the tower bending moments in both operating regions below and above rated wind speed. Furthermore, it is indicated that the estimation of blade related loads is possible as well, albeit to a much lesser extent.

There are a lot of publications dealing with simulations of load reducing control systems. A few concern field tests with wind turbines in the class below 1MW, see for example [13],[14],[15]. But, to the authors' knowledge, no field tests have been reported so far on large-scale systems.

Results of preparatory work are also given. Section 2.1 describes a simple model for the longitudinal motion of the tower and section 4.1 deals with estimation results regarding that model. This approach is more in the line of the approach in [5] where the aerodynamic thrust force is an input of the tower model. These sections can be skipped without loss by those only interested in the main results.

The report closes with general conclusions in section 5.

Remark: Please note that sensitive data regarding the wind turbine used in the field test is obliterated throughout the text. For example, frequency related values are normalized with the rotor speed.

2 Wind turbine and wind speed models

This section describes the models used below. The first subsection is about a model of the longitudinal tower motion that has been employed for a preliminary study and is very similar to the approach in [5]. It is closely related to the results presented in section 4.1 but only loosely connected with the main results, and, therefore, can be skipped by those only interested in the main results. The model of the whole wind turbine, which has been used to obtain the main results, is described in section 4.2. Both models rely on measurement or estimation of the wind speed. Two different methods for wind speed estimation are given in the last subsection.

2.1 Simple longitudinal tower model

The origin of this model can be found in [5] where tower models based on modal analysis are excited by the aerodynamic thrust force to estimate the tower bending moment. Although this report focuses on the model described in the subsequent section the results regarding the simple model are interesting in two respects. Firstly, they can be seen as a verification of the simple multi-body approach, and secondly, they give additional insight.

The simple model of the longitudinal tower motion are two rigid beams connected with spring/damper pairs, see Figure 1. Thus, the first and the second tower mode are approximated. Constructive data is used for the calculation of the inertia, the mass, the centre of mass, etc. while the nacelle and the rotor are assumed to be point masses on top of the second beam element. For the adjustment of the parameters of the springs and dampers according to the eigenfrequencies and damping see section 4.1.2.

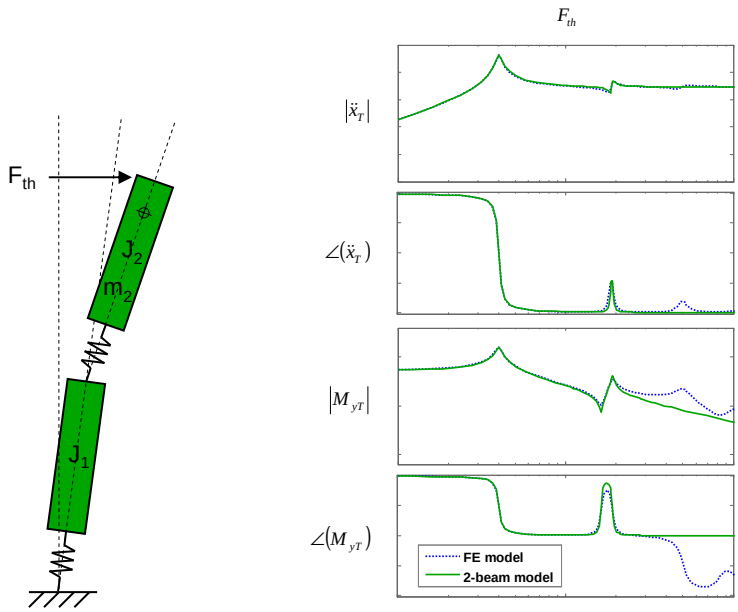

Figure 1: Simple model of the longitudinal tower motion. The bode plots show the frequency-response from the thrust force to the tower top acceleration and the tower bending moment. Green: simple model. Blue, dotted: finite element model.

On top of the second element the aerodynamic thrust force F_{th} is assumed to excite the structure. The model's outputs are the tower top acceleration $\ddot{x}_T$ and the tower bending moment M_{yT}, i.e. the acceleration at the top of the second element and the bending moment of

the spring between the elements. This output configuration fits to the sensor configuration of the results reported in section 4.

A finite element model consisting of 30 linear Euler-Bernoulli beams is defined to validate the simple approach. The FE-model's parameters are directly obtained from the constructive data of the tower. On the right hand side in Figure 1 the frequency-responses of this model and the simple model are shown. The responses fit almost exactly up to the second mode. In the context of this work, this is assumed to be sufficient.

2.2 Full model

The full model is a model of the whole 3-bladed wind turbine. This model has been developed at Fraunhofer IWES especially for control design [6] and is similar to the model from [7].
It is a linear time-invariant state-space model for a distinct operating point, which is determined by the mean wind speed. The numerical state-space model is automatically derived by a software routine in Matlab, see [6] for a detailed description.

Structural dynamics

The structural dynamics of the wind turbine are approximated by a linearized multibody system. This system consists of a number of rigid beam elements, which are connected by joints. Every joint consists of a spring/damper pair to emulate the spatial distributed stiffness and damping properties of the whole structure. A minimum number of elements is intended to keep the system order as low as possible.

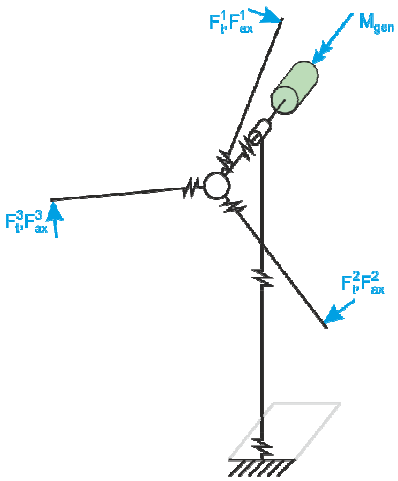

Figure 2: Mechanical structure of the full model.

Figure 2 shows the chosen mechanical structure. The tower is approximated by two elements with a longitudinal and a lateral degree of freedom each. On top of the tower is the shaft with a single rotational degree of freedom. It is connected to the generator and the blades. The blades have an edgewise and a flapwise degree of freedom each. Thus, the model has the following structural modes:

- 1st and 2nd tower fore-aft and side-side bending modes,
- 1st flapwise and edgewise bending modes, and
- 1st drive train torsion mode.

In a steady operating point the constant rotation speed leads to equations that are periodic. To eliminate this periodicity, the multiblade or Colman transformation is used [9]. This transformation[1] maps physical quantities related to the three blades to an abstract space with a collective, a sine and a cosine coordinate. In the following, the indices 0, s and c refer to these coordinates.

[1] A formally equal transformation is the d-q-axis transformation commonly used for 3 phase electrical machines.

Aerodynamics and overall system

As it is shown in Figure 2, the aerodynamic forces are assumed to attack at a single point on each blade. The forces are determined using the c_P-λ and c_T-λ characteristics of the rotor depending on the pitch angle. Linearization is obtained by computing their partial derivatives with respect to pitch angle, wind speed and rotor speed. A feedback from the mechanical structure to the wind field is realised by calculating an effective wind speed at the blades in multiblade coordinates: the effective wind speed is the free, local wind speed less the velocity of the structure at the force application point.

Once again, to keep the number of states low and the model simple, dynamic inflow effects are neglected as well as the pitch and generator actuators dynamics. A proportional feedback of the generator speed to generator torque is applied in the operating region below rated wind speed. This constant is adjusted with respect to the slope of the generator's speed-torque characteristic at the particular operating point. The PI-controller of the pitch control loop of the field test wind turbine is applied in the region above rated wind speed.

The resulting closed-loop system is then defined by

$$\begin{aligned} \dot{\mathbf{x}} &= \mathbf{A}\,\mathbf{x} + \mathbf{B}\,\mathbf{u}, \\ \begin{bmatrix} \mathbf{y}_m \\ \mathbf{y}_p \end{bmatrix} &= \begin{bmatrix} \mathbf{C}_m \\ \mathbf{C}_p \end{bmatrix} \mathbf{x} + \begin{bmatrix} \mathbf{D}_m \\ \mathbf{D}_p \end{bmatrix} \mathbf{u}, \end{aligned} \tag{2.1}$$

where the input vector

$$\mathbf{u} = \begin{bmatrix} v_0 & v_s & v_c \end{bmatrix}^T$$

contains the wind speed, the output signals are the measured signals

$$\mathbf{y}_m = \begin{bmatrix} \ddot{x}_T & \ddot{y}_T & \Omega & \theta_0 \end{bmatrix}^T$$

and the bending moments

$$\mathbf{y}_p = \begin{bmatrix} M_{yT} & M_{xT} & M_{fl,0} & M_{fl,s} & M_{fl,c} & M_{ed,0} & M_{ed,s} & M_{ed,c} \end{bmatrix}^T,$$

which have to be estimated by the state observer described below. See Table 1 for the description of the signals. The states of the model are deflections of the angles and angular velocities between the beam elements from their constant operating point values. Note that there is a direct feedthrough to the tower top accelerations and the blade bending moments, i.e. the corresponding matrices in Eq. (2.1) are not equal to zero.

v_0, v_s, v_c	wind speed in multiblade coordinates
$\ddot{x}_T$	longitudinal tower top acceleration
$\ddot{y}_T$	lateral tower top acceleration
Ω	rotor speed
θ_0	collective pitch angle
M_{yT}	longitudinal tower bending moment
M_{xT}	lateral tower bending moment
$M_{fl,0}, M_{fl,s}, M_{fl,c},$	flapwise blade bending moment in multiblade coordinates
$M_{ed,0}, M_{ed,s}, M_{ed,c}$	edgewise blade bending moment in multiblade coordinates

Table 1: Inputs and outputs of the full model.

As already mentioned, the state-space model in Eq. (2.1) is automatically derived by a software routine. To this end, the inertia related parameters of the mechanical parts, i.e. the beam

elements, are taken from constructive data. The stiffness and damping parameters are adjusted so that the modal frequencies and damping fit to the results obtained from operational modal analysis [16].

2.3 Wind speed

An estimation of the current wind speed is needed for both models. For the longitudinal tower model the thrust force input is calculated on basis of the estimated wind speed. In case of the full model the wind speed is directly used as an input of the system.

Two different methods for wind speed estimation are investigated:

- external estimation, where the measured values of the rotor speed, the electrical power and the collective pitch angle are used to calculate the current wind speed, and
- internal estimation, where the wind speed is modelled by a linear time-invariant system and is estimated by an input signal observer.

The word “internal” refers to the integration of the wind speed estimation into an overall observer consisting of both state and input signal observer – in contrast to the “external” estimation, which is fed into the state observer as an input signal.

2.3.1 External estimation by measured values and power coefficient

Assuming the wind speed to be uniformly distributed over the rotor area an established method is to use the measured values and the aerodynamics of the rotor to reconstruct the wind speed, see e.g. [1] and [3]. The relation between wind power captured by the rotor P_R and wind speed v is given by

$$P_R = \frac{\rho}{2} A_R v^3 c_P\left(\frac{\Omega \cdot R}{v}, \theta_0\right), \tag{2.2}$$

where Ω is the rotor speed, R is the rotor radius, A_R is the rotor area, θ_0 is the collective pitch angle, ρ is the density of the air, and $c_P(\cdot,\cdot)$ is the power coefficient.

However, not the rotor power is measured but the electrical power of the generator P_{el}, which is only a low-frequency estimation of the rotor power due to the power that is buffered in the rotor an the drive train. Neglecting drive train modes the rotor power is better approximated by the sum of the electrical power without generator losses and the power that accelerates the rotor:

$$\tilde{P}_R = \frac{P_{el}}{\eta_{el}} + J_R \dot{\Omega}, \tag{2.3}$$

where J_R is the rotor inertia and η_{el} is the power efficiency of the generator.

Eqs. (2.2) and (2.3) do not define v uniquely as a function of the measured values. For example, there is a “pre-stall” and a “post-stall” solution with a low and a high value of v. Since we are dealing with variable speed wind turbines, only the pre-stall solution is of significance and the others have to be ignored. For the online estimation of the wind speed a 3-dimensional lookup-table is generated:[2]

$$\tilde{v} = f\left(\tilde{P}_R, \Omega, \theta_0\right),$$

where $\tilde{P}_R$ is calculated using Eq. (2.3).

[2] Solving the implicit definition of v online is also possible [1] , [3].

Because the wind speed is assumed to be uniformly distributed over the rotor area we define $\tilde{v}_0 = \tilde{v}$ and the asymmetric parts of the wind speed are set to zero. This model, therefore, does not allow for the integration of spatially distributed effects.

2.3.2 Internal estimation by observer

The term “internal wind speed estimation” refers to the estimation of an input signal by a linear state observer. For this purpose a linear time-invariant model of the signal has to be chosen. Its states are estimated together with the states of the model of the system that is driven by the input signal. This is described more fully in section 3.

A very general approach to account for different effects is a system driven by a white noise input vector $\boldsymbol{\mu}_d$:

$$\begin{aligned} \dot{\mathbf{x}}_d &= \mathbf{A}_d \mathbf{x}_d + \boldsymbol{\mu}_d, \\ \mathbf{u} &= \mathbf{C}_d \mathbf{x}_d, \end{aligned} \tag{2.4}$$

where $\mathbf{u} = \begin{bmatrix} v_0 & v_s & v_c \end{bmatrix}^T$ is the input vector of system (2.1), i.e. the wind speed in multiblade coordinates. The number of states and the matrices depend on the signal model.

This approach is quite flexible because it can model spatially distributed stochastic and deterministic effects. However, this flexibility has not been used for the estimation results presented in section 4.2. The best results were obtained using nothing more than a single integrator for the collective part, i.e. setting

$$\mathbf{A}_d = 0, \qquad \mathbf{C}_d = \begin{bmatrix} 1 & 0 & 0 \end{bmatrix}^T. \tag{2.5}$$

More sophisticated models have not been studied closer because of two main reasons. Firstly, with more complex models the observer design can become quite a challenge. From a practical point of view this is undesirable. Secondly, the results presented below suggest that there are issues related to the asymmetric rotor components. For example, the chosen configuration of measurement signals is not likely to be well suited to observe asymmetric, rotor related effects. More detailed comments on observability are made in the next section.

3 Observer

A state space observer is used to estimate both the states of the wind turbine model and the states of the wind speed model. Observers have also been used in the preceding work [5]. The following two sections describe the structure and the design methodology, which are in line with the notion of linear-quadratic estimation and the Kalman-Bucy filter [1]. Furthermore, comments on the observability of the states of the model are given.

3.1 Structure

Figure 3 shows the structure of the overall linear model comprising the wind speed and the wind turbine model and the observer. A tilde above a symbol refers to estimated values. The derivation of the model equations for the design of the observer feedback matrix is given step by step.

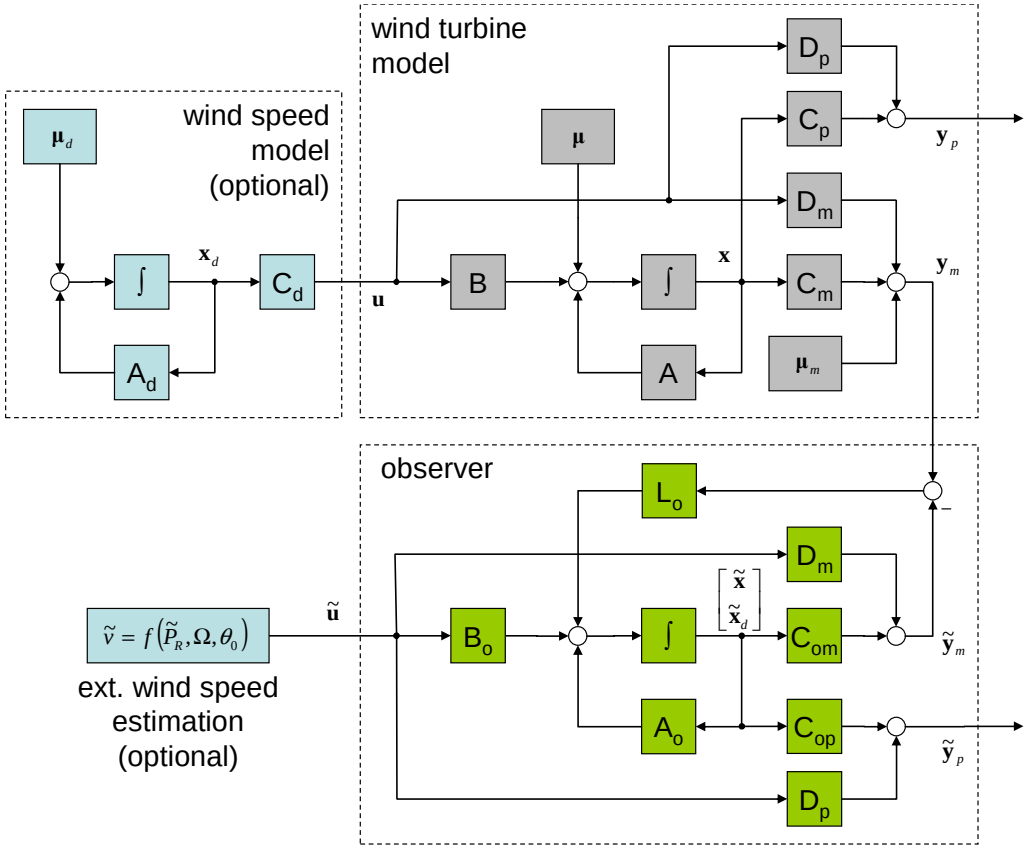

Figure 3: Block schematic of the overall structure. The wind speed input depends on the chosen wind speed estimation method.

The input and output signals of the wind turbine model in Eq. (2.1) are different physical quantities with quite different orders of magnitude. Hence, all the signals are being normalized so the state-space equations are properly scaled. Note that, in what follows, this assumption is very important.

Furthermore, the wind turbine model from Eq. (2.1) is extended by two vectors $\boldsymbol{\mu}$ and $\boldsymbol{\mu}_m$ containing zero-mean white noise, which can be interpreted as uncertainties in the turbine model and the measurement signals:

$$\begin{aligned}\dot{\mathbf{x}} &= \mathbf{A}\mathbf{x} + \mathbf{B}\mathbf{u} + \boldsymbol{\mu},\\ \mathbf{y}_m &= \mathbf{C}_m\mathbf{x} + \mathbf{D}_m\mathbf{u} + \boldsymbol{\mu}_m,\\ \mathbf{y}_p &= \mathbf{C}_p\mathbf{x} + \mathbf{D}_p\mathbf{u}.\end{aligned} \tag{3.1}$$

The reason for this extension becomes clear in the next section, where the covariance matrices of $\boldsymbol{\mu}$ and $\boldsymbol{\mu}_m$ are meaningful parameters for the design of the feedback matrix. Eq. (3.1) is used for the design of the observer feedback matrix $\mathbf{L}_o$ with external wind speed estimation. We get the equation for the design with internal wind speed estimation after inserting the wind speed model from Eq. (2.4) in Eq. (3.1):

$$\begin{aligned}\begin{bmatrix}\dot{\mathbf{x}}\\ \dot{\mathbf{x}}_d\end{bmatrix} &= \begin{bmatrix}\mathbf{A} & \mathbf{B}\mathbf{C}_d\\ \mathbf{0} & \mathbf{A}_d\end{bmatrix}\begin{bmatrix}\mathbf{x}\\ \mathbf{x}_d\end{bmatrix} + \begin{bmatrix}\boldsymbol{\mu}\\ \boldsymbol{\mu}_d\end{bmatrix},\\ \mathbf{y}_m &= \begin{bmatrix}\mathbf{C}_m & \mathbf{D}_m\mathbf{C}_d\end{bmatrix}\begin{bmatrix}\mathbf{x}\\ \mathbf{x}_d\end{bmatrix} + \boldsymbol{\mu}_m,\\ \mathbf{y}_p &= \begin{bmatrix}\mathbf{C}_p & \mathbf{D}_p\mathbf{C}_d\end{bmatrix}\begin{bmatrix}\mathbf{x}\\ \mathbf{x}_d\end{bmatrix}.\end{aligned} \tag{3.2}$$

In the same manner as before $\boldsymbol{\mu}_d$ can be interpreted as a model uncertainty during the design process – although it has been introduced in section 2.3.2 for a different purpose.

The equations of the observer part in Figure 3 are

$$\begin{aligned}\begin{bmatrix}\dot{\tilde{\mathbf{x}}}\\ \dot{\tilde{\mathbf{x}}}_d\end{bmatrix} &= \mathbf{A}_o\begin{bmatrix}\tilde{\mathbf{x}}\\ \tilde{\mathbf{x}}_d\end{bmatrix} + \mathbf{B}_o\tilde{\mathbf{u}} + \mathbf{L}_o\left(\mathbf{y}_m - \tilde{\mathbf{y}}_m\right),\\ \tilde{\mathbf{y}}_m &= \mathbf{C}_{o,m}\begin{bmatrix}\tilde{\mathbf{x}}\\ \tilde{\mathbf{x}}_d\end{bmatrix} + \mathbf{D}_m\tilde{\mathbf{u}},\\ \tilde{\mathbf{y}}_p &= \mathbf{C}_{o,p}\begin{bmatrix}\tilde{\mathbf{x}}\\ \tilde{\mathbf{x}}_d\end{bmatrix} + \mathbf{D}_p\tilde{\mathbf{u}}.\end{aligned} \tag{3.3}$$

For the internal wind speed estimation we set $\tilde{\mathbf{u}} = \mathbf{0}$ and the matrices are determined according to the combination of the wind turbine and the wind speed model, i.e.

$$\mathbf{A}_o = \begin{bmatrix}\mathbf{A} & \mathbf{B}\mathbf{C}_d\\ \mathbf{0} & \mathbf{A}_d\end{bmatrix}, \qquad \mathbf{C}_{o,m} = \begin{bmatrix}\mathbf{C}_m & \mathbf{D}_m\mathbf{C}_d\end{bmatrix},\ \mathbf{C}_{o,p} = \begin{bmatrix}\mathbf{C}_p & \mathbf{D}_p\mathbf{C}_d\end{bmatrix}. \tag{3.4}$$

In case of the external wind speed estimation the matrices are simply equal to those of the wind turbine model.

Observability

For the design of the observer feedback matrix $\mathbf{L}_o$ the pair $\left(\mathbf{A}_o, \mathbf{C}_{o,m}\right)$ must be observable. That is, the models of wind turbine and wind speed have to fit to the sensor configuration. Here, with measurement configuration chosen in section 2.2, i.e. tower top acceleration, rotor speed,

and collective pitch angle, and the simple wind speed model from Eq. (2.5) the pair $(\mathbf{A}_o, \mathbf{C}_{o,m})$ is observable.

If, for example, it is intended to model a yaw misalignment by a constant deflection in the sine coordinate of the wind speed this is not to be seen from the measured outputs of the wind turbine model in section 2.2. It would, however, be seen from the flapwise blade bending moments. In the terminology of control theory: the corresponding integrator in the wind speed signal model must be observable from the output signals of the overall model.

It is interesting to note that integrators modelling asymmetric wind speed components are observable using measurements of the tower bending moments. This means that, in principle, it is not impossible to observe low frequency asymmetric rotor effects from the tower bending moments. Since strain gauges are much easier attached to the tower than to the blades, let alone maintenance, this suggests an interesting application. Admittedly, these sensors have issues in the low frequency range because of drift. Therefore, the potential of this approach is not studied further here but can be subject of future works.

3.2 Design

The observer design is the determination of the observer feedback matrix $\mathbf{L}_o$. For the Kalman-Bucy filter the formal objective is the minimization of the variance of the state estimation error subject to the model uncertainties. For this purpose the covariance matrices $\boldsymbol{\Sigma}, \boldsymbol{\Sigma}_d$, and $\boldsymbol{\Sigma}_m$ of the model uncertainties $\boldsymbol{\mu}, \boldsymbol{\mu}_d$, and $\boldsymbol{\mu}_m$ have to be defined. To keep things simple, they are defined as diagonal matrices with equal elements:

$$\boldsymbol{\Sigma} = \sigma^2 \mathbf{I}, \qquad \boldsymbol{\Sigma}_d = \sigma_d^2 \mathbf{I}, \qquad \boldsymbol{\Sigma}_m = \mathbf{I}, \tag{3.5}$$

where $\mathbf{I}$ denotes identity matrices of appropriate size, and the scalar values σ and σ_d are the actual design parameters. Of course the second parameter is omitted in case of the external wind speed estimation.

Adjusting these parameters can be interpreted as balancing the confidence one has in the different models. This is not an easy task, since there is no absolute measure for their uncertainty.

One way is to evaluate the closed-loop transfer function matrix $\mathbf{G}_m(s)$ from the actual measurement vector $\mathbf{y}_m$ to the estimated measurement vector $\tilde{\mathbf{y}}_m$ after computing the observer feedback matrix $\mathbf{L}_o$. This is exemplified in Figure 4, where the amplitude response in the upper left corner of $\mathbf{G}_m(s)$ is shown for two different choices of σ in case of external wind speed estimation. For the blue and the green, dotted line the parameter is set to $\sigma = 100$ and $\sigma = 1$, respectively. It is obvious from the diagonal elements that the first choice is much more sensible: the amplitude is near 0dB for low frequencies. Further increasing the parameter, i.e. declining confidence in the turbine model and more confidence in the measurement, leads to an even tighter coupling between $\mathbf{y}_m$ and $\tilde{\mathbf{y}}_m$. But then other effects like the peaking phenomenon have to be taken into account as well.

In case of the internal wind speed estimation the resulting estimated wind speed has to be monitored carefully. Too high values of σ_d lead to noisy wind speed estimations with unrealistically high amplitudes.

For the estimation results given in section 4.2 the design parameters have been chosen

- $\sigma = 100$ for the external wind speed estimation and
- $\sigma = 10, \sigma_d = 100$ for the internal wind speed estimation.

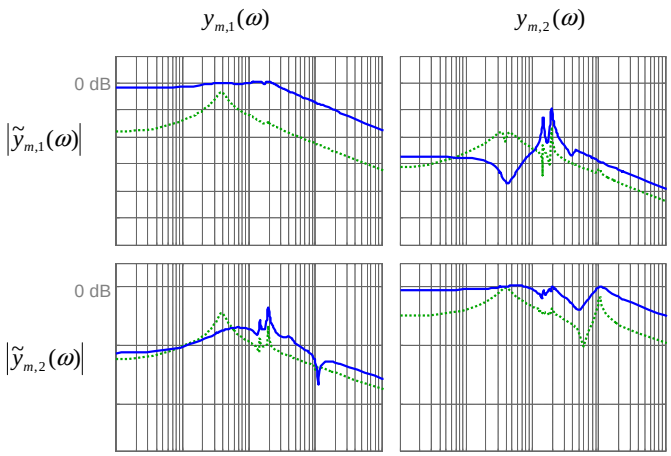

Figure 4: Amplitude response of the 2x2 upper left corner of $\mathbf{G}_m(s)$ for two different design parameters. Blue: $\sigma = 100$. Green, dotted: $\sigma = 1$.

4 Field test – estimation results

This section presents estimation results using field test data from a commercial 5MW turbine [7]. It is divided in two subsections. The first one deals with the simple longitudinal tower model and can be skipped without loss if only the main results are of interest. These are given in the second subsection. Before that, the field test configuration and the validation measures are described briefly.

The field test data is obtained from a wind turbine that is equipped with strain gauges mounted on the tower centre at 60 m height measuring the tower bending moments. At the blade roots strain-gauge sensors measure flapwise and edgewise blade bending moments. These quantities related to each individual blade are transformed into a non-rotating frame using the multiblade transformation. From the operating control system we get measurements of the tower top accelerations, the collective pitch angle, and the rotor speed.

For the validation of the estimation results the measured and the estimated time series are compared both in the time and in the frequency domain. For a condensed view we use the normalized mean square error, which is defined by

$$\mathrm{NMSE}(x) = \frac{\mathrm{var}(x_{meas} - x_{est})}{\mathrm{var}(x_{meas})}. \tag{4.1}$$

In section 4.2, where the main results are presented, a closer look is taken to the fatigue loads of the tower. Rainflow counting is processed on the time series and damage equivalent loads are computed by

$$\mathrm{A}_{DEL} = \left(\sum_i \frac{A_i^m n_i}{n_{ref}} \right)^{\frac{1}{m}}, \tag{4.2}$$

where A_i and n_i are the stress amplitude and its number of cycles, the equivalent number of cycles $n_{ref} = 10^8$, and the Wöhler curve exponent $m = 4$. It has shown to be more meaningful to perform the rainflow counting on low pass filtered versions of the time series while steadily increasing the cut-off frequency. The resulting spectra give information about which frequency contents are critical.

4.1 Longitudinal tower model

This section contains the results related to the longitudinal tower model. As it has already been pointed out above, these results should be seen as preparatory work for the actual main results presented in the subsequent section. Although they do not lead to the main results in a straight forward manner they are included here because they give additional insight.

4.1.1 Thrust Force estimation

The input of the longitudinal tower model is the aerodynamic thrust force, which is not measured directly and, therefore, has to be estimated using the mean wind speed. As the accelerometer is an inaccurate representation of the spatial and temporal mean wind speed it has to be estimated as well. This can be done using the external method described in section 2.3.1. The thrust force is then computed using the c_T-λ characteristics of the rotor.

Figure 5 shows a comparison of the wind speed measured by the anemometer and estimated by the external estimation, for both below and above rated wind speed. There is a fair correlation between both signals. The external wind speed estimation is smoother – probably because it is a

spatial average over the whole rotor plane – and more likely to represent the actual mean wind speed. This conjecture is supported by the results according to thrust force and tower bending moment reported below.

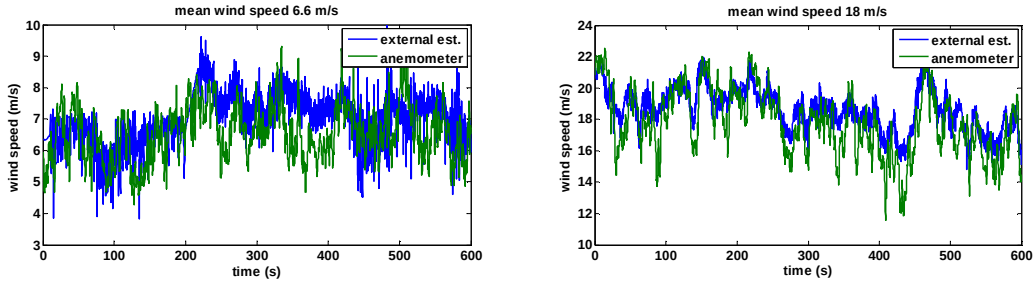

Figure 5: Comparison of wind speed measured by the anemomenter (blue) and estimated by the method described in section 2.3.1. Left: 6 m/s mean wind speed. Right: 18 m/s mean wind speed.

Another interesting way to estimate the thrust force is to use the measurement of the flapwise blade bending moments. Of course, this is for comparison purposes only as, from a practical point of view, it is not sensible to measure blade bending moments for the estimation of the tower bending moments. It would be much easier to attach sensors to the tower than to the blades.

For this comparison method, the thrust force is assumed to be proportional to the collective flapwise blade bending moment

$$F_{th} = \frac{1}{r_{Fax}} M_{fl,0}, \tag{4.3}$$

where the proportionality factor $1/r_{Fax}$ is adjusted manually according to the overall estimation results.

Figure 6 compares the thrust force estimation in time and frequency domain using the different methods, again for both below and above rated wind speed. Only the deflections from the mean value are shown.

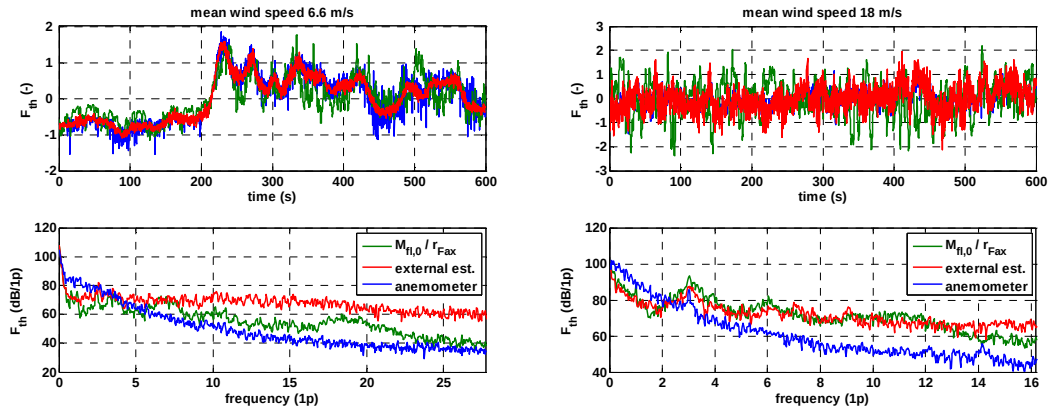

Figure 6: Comparison of the thrust force estimated using the anemometer measurement (blue), the external wind speed estimation (red), and the assumption that $F_{th} = M_{fl,0}/r_{Fax}$ (green). The upper and lower plots show the signals in the time and the frequency domain, respectively. Left: 6 m/s mean wind speed. Right: 18 m/s mean wind speed.

There is a good correlation between very slowly varying components for 6 m/s mean wind speed. This holds true for the external estimation and the comparison method using the blade bending moments for 18 m/s mean wind speed. In that operating region both methods fit not bad in the frequency domain up to 10p. Harmonics of the rotor speed are clearly present.

In general, the anemometer based estimation “overdoes it” in the low frequency and understates the higher frequencies. This is in line with the temporal low pass characteristic of the cup anemometer and its lack of spatial averaging over the rotor plane. Structural effects can not be identified.

4.1.2 Tower bending moment estimation

The thrust force estimated by three different methods are now applied to the longitudinal tower model. To this end, the damping values of the tower model have to be adjusted according to the approach.

That is, for the anemometer and the external wind speed estimation based methods the logarithmic decrement is chosen 0.8 and 0.3 for the 1^{st} and the 2^{nd} tower bending mode, respectively. This is due to the high aero-dynamic damping of the longitudinal tower motion. For the method using the collective blade bending moment, the aero-dynamic damping is effectively inherent in the measurement signal. Therefore, the best results are obtained using significantly lower logarithmic decrements: 0.06 and 0.15. The eigenfrequencies are adjusted according to the results of an operational modal analysis [16].

Figure 7 to Figure 10 show the estimation results in time and frequency domain using the different methods.[3] In Table 2 the corresponding normalized mean square errors are summarized. There are transient effects because the models initial state are not corresponding to the “real” initial state. The models eigenvalues are all located in the open left complex half plane. Hence, these effects decay and the normalized mean square error is calculated using the second half of the 10 min data sequence. Thus, all transient effects are excluded.

The comparison method using the collective blade bending moment is enhanced by an additional input at top of the longitudinal tower model. More precisely, the cosine part of the blade bending moment is applied to the top of the second beam element. As given in Table 2 this further enhances the estimation result.

The main findings are as follows.

The method based on the anemometer measurement is totally unsatisfying, which is in line with the remarks in the preceding pages. From the frequency domain plots in Figure 8 and Figure 10 it can be observed that only in the range of the first tower mode there is some correlation between measurement and estimation. Below this range the effect of overestimating the wind speed, which is described in the previous section, is clearly to be seen in the estimation of the tower bending moment.

Estimating the thrust force based on the external estimation does a lot better. Although the longitudinal tower top acceleration is not properly reproduced, the normalized mean square error of the tower bending moment indicates quite good correlation between measurement and estimation.

The comparison method based on the measurement of the flapwise bending moment leads to the most accurate estimation results. An interesting observation is the further improvement that

[3] Time and frequency domain plots of the comparison method using only the collective blade bending moments are not shown.

is achieved by using both collective and cosine part of the flapwise bending moment, see the last four columns in Table 2.

As mentioned before, this method is not directly usable in practice. However, it can be useful for the estimation of the collective blade bending moment if the inverse transfer function is regarded with the longitudinal tower bending moment as an input. Or an observer employing the measurement of the tower top acceleration can be used, see [5] for this approach. However, these issues are not investigated further here, since they only deal with the longitudinal motion.

approach	*anemometer measurement*		*external wind speed estimation*		*flapwise bending moment (collective & cosine)*		*flapwise bending moment(only collective)*	
mean wind speed	*6 m/s*	*18 m/s*	*6 m/s*	*18 m/s*	*6 m/s*	*18 m/s*	*6 m/s*	*18 m/s*
NMSE($\ddot{x}_T$)	2.28	1.53	1.82	0.759	0.461	0.565	0.667	0.795
NMSE(M_{yT})	1.5	3.58	0.357	0.548	0.108	0.365	0.19	0.625

Table 2: Comparison of the normalized mean square errors[*)] (NMSE) of the estimated longitudinal tower top acceleration and bending moment.

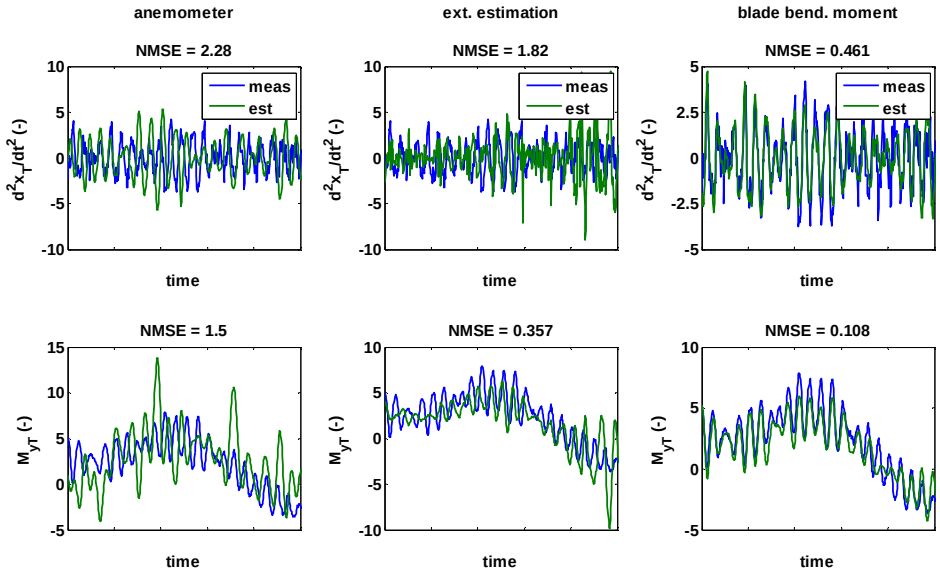

Figure 7: Sections of the time domain plots of the measured (blue) and estimated (green) signals at 6 m/s mean wind speed. The upper and lower plots show the tower top acceleration and the tower bending moment, respectively. The given values of the NMSE[*)] are calculated for the second half of the 10 min data sequence. The thrust force is caculated using three different approaches. Left: anemometer measurement. Middle: external wind speed estimation. Right: flapwise blade bending moment.

[*)] see Eq. (4.1)

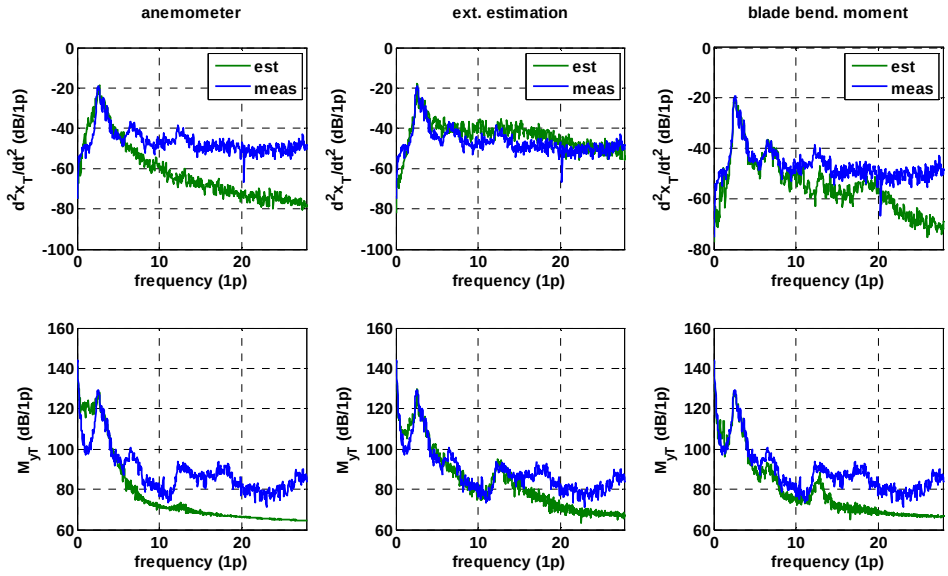

Figure 8: Frequency domain plots of the measured (blue) and estimated (green) signals at 6 m/s mean wind speed. The upper and lower plots show the tower top acceleration and the tower bending moment, respectively. The thrust force is caculated using three different approaches. Left: anemometer measurement. Middle: external wind speed estimation. Right: flapwise blade bending moment.

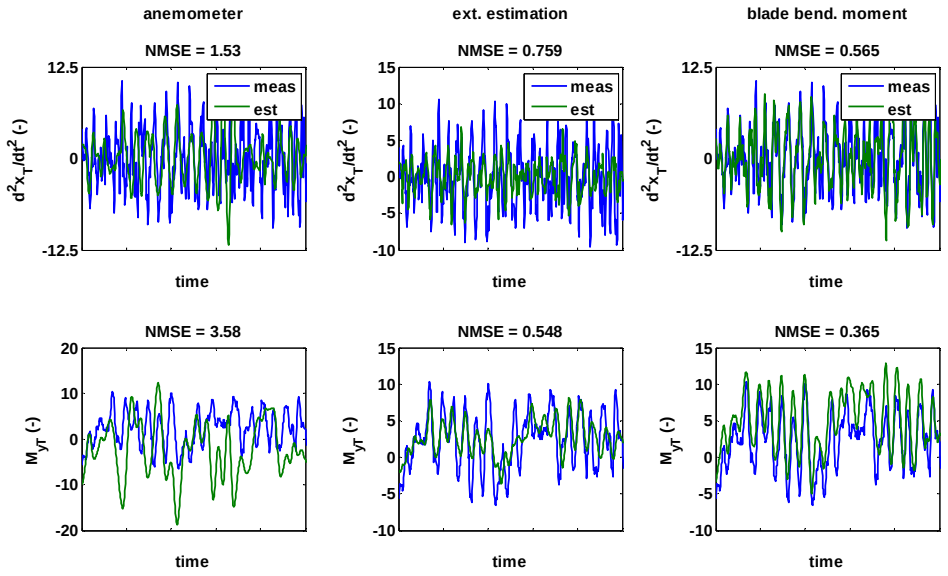

Figure 9: Sections of the time domain plots of the measured (blue) and estimated (green) signals at 18 m/s mean wind speed. The upper and lower plots show the tower top acceleration and the tower bending moment, respectively. The given values of the NMSE*) are calculated for the second half of the 10 min data sequence. The thrust force is caculated using three different approaches. Left: anemometer measurement. Middle: external wind speed estimation. Right: flapwise blade bending moment.

*) see Eq. (4.1)

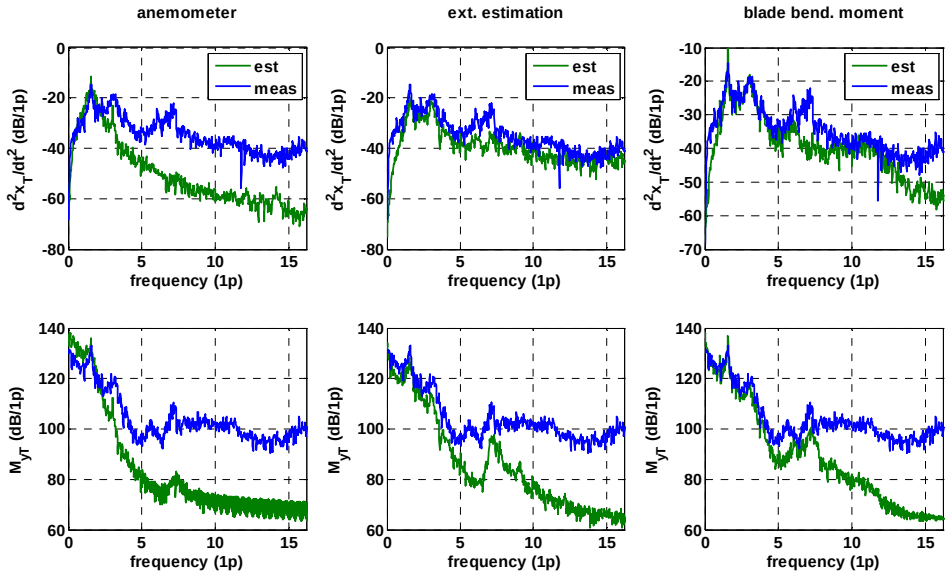

Figure 10: Frequency domain plots of the measured (blue) and estimated (green) signals at 18 m/s mean wind speed. The upper and lower plots show the tower top acceleration and the tower bending moment, respectively. The thrust force is caculated using three different approaches. Left: anemometer measurement. Middle: external wind speed estimation. Right: flapwise blade bending moment.

4.2 Full model

In the following three subsections the main results of this work are presented. That is, the full model is used with measurement of the tower top accelerations, the collective pitch angle and the rotor speed. Both internal and external wind speed estimation are considered. The first subsection summarises the estimation of the tower bending moment. Then the two different wind speed estimations are compared. Eventually, the section closes with results concerning blade bending moments.

4.2.1 Tower bending moment estimation

In Figure 11 to Figure 14 there are shown the results of the tower bending moment estimation for 6 and 18 m/s mean wind speed using the internal and the external wind speed estimation. For longitudinal and lateral motion each figure contains time and frequency domain plots and a plot of the frequency depending load equivalent.[4] The corresponding normalized mean square errors are summarised in Table 3, where the results with the longitudinal model and external wind speed estimation from Table 2 are given for comparison.

Looking at the time domain plot in the figures and at the normalized mean square errors in the table we find that in the range below rated wind speed the results obtained using the external wind speed estimation are slightly better than the results obtained with internal wind speed estimation. In the range above rated wind speed it is the other way around. Compared to the longitudinal model the results obtained with the full model and internal estimation are better in both regions. The results obtained with the full model and external estimation are better below rated and marginally worse above rated wind speed.

For the frequency domain plots and the frequency depending damage equivalent loads the following conclusions can be drawn.

[4] See Eq. (4.2) and the following for the definition of the frequency depending damage equivalent load.

All the frequency depending damage equivalent load of the measurements – the longitudinal bending moment at 18 m/s being an exception – show two steps: a first at the very low frequencies and a second at the first tower mode. While the first is not properly reproduced by both wind speed estimation methods, the second is present with appropriate height in all plots.

The estimated lateral bending moment is noisy at frequencies above the first tower bending mode. At 18 m/s mean wind speed, this causes a third step in the frequency depending damage equivalent load at 3p frequency, which is not present in the actual measurement. Below the first tower bending mode the estimated signals are too weak. The latter might be because yaw misalignment which is not included in the model.

The best result so far is obtained for the longitudinal bending moment in above rated wind speeds using the internal wind speed estimation. In the lower left subplot in Figure 12 the shape of the damage equivalent load curve fits quite well. In contrast to this, using the external wind speed estimation leads to much worse results in that case.

approach	*full model, internal wind speed estimation*		*full model, external wind speed estimation*		*longitudinal model, external wind speed estimation*	
mean wind speed	*6 m/s*	*18 m/s*	*6 m/s*	*18 m/s*	*6 m/s*	*18 m/s*
NMSE(M_{yT})	0.219	0.288	0.139	0.57	0.357	0.548
NMSE(M_{xT})	0.353	0.363	0.298	0.407	-/-	-/-

Table 3: Comparison of the normalized mean square errors*) (NMSE) of the estimated tower bending moments. The values for the longitudinal model have been taken from Table 2 for comparison.

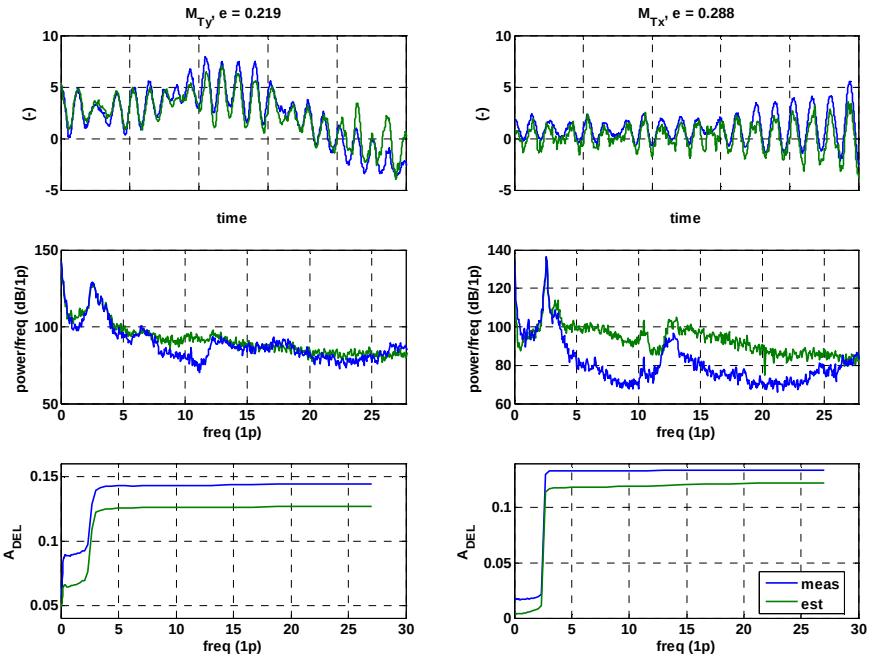

Figure 11: Longitudinal (left) and lateral (right) tower bending moment measurement (blue) and estimation with *internal* wind speed estimation (green) at *6 m/s mean wind speed*. Top: time domain, center: frequency domain, bottom: frequency depending damage equivalent load. The normalized mean square error*) of the whole sequence is given in the title of the time domain plot.

*) see Eq. (4.1)

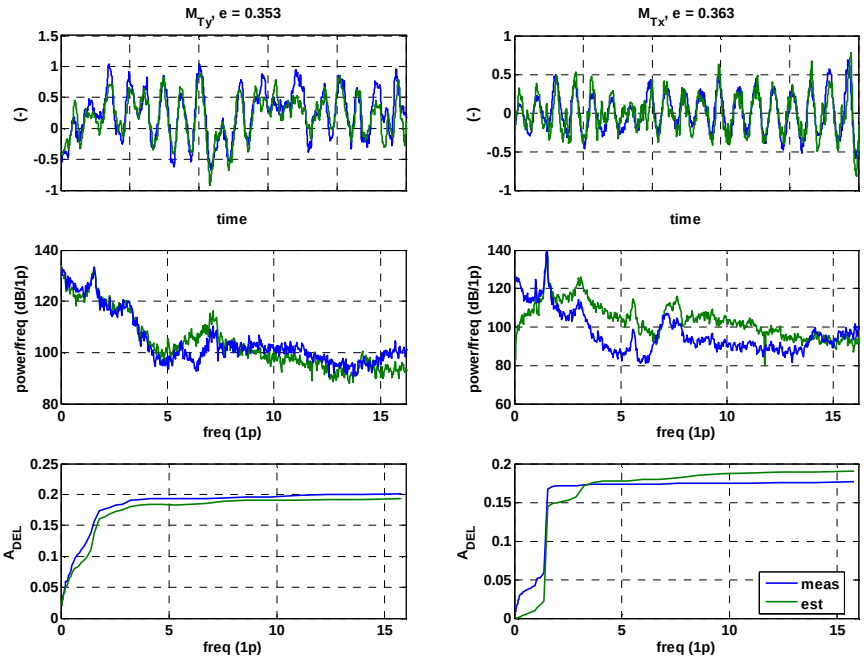

Figure 12: Longitudinal (left) and lateral (right) tower bending moment measurement (blue) and estimation with *internal* wind speed estimation (green) at *18 m/s mean wind speed*. Top: time domain, center: frequency domain, bottom: frequency depending damage equivalent load. The normalized mean square error*) of the whole sequence is given in the title of the time domain plot.

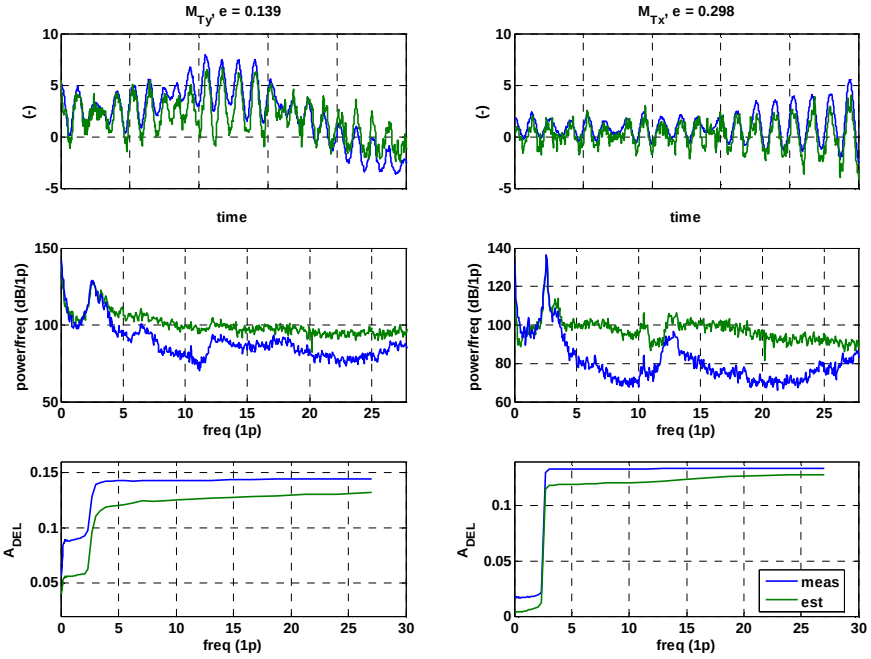

Figure 13: Longitudinal (left) and lateral (right) tower bending moment measurement (blue) and estimation with *external* wind speed estimation (green) at *6 m/s mean wind speed*. Top: time domain, center: frequency domain, bottom: frequency depending damage equivalent load. The normalized mean square error*) of the whole sequence is given in the title of the time domain plot.

*) see Eq. (4.1)

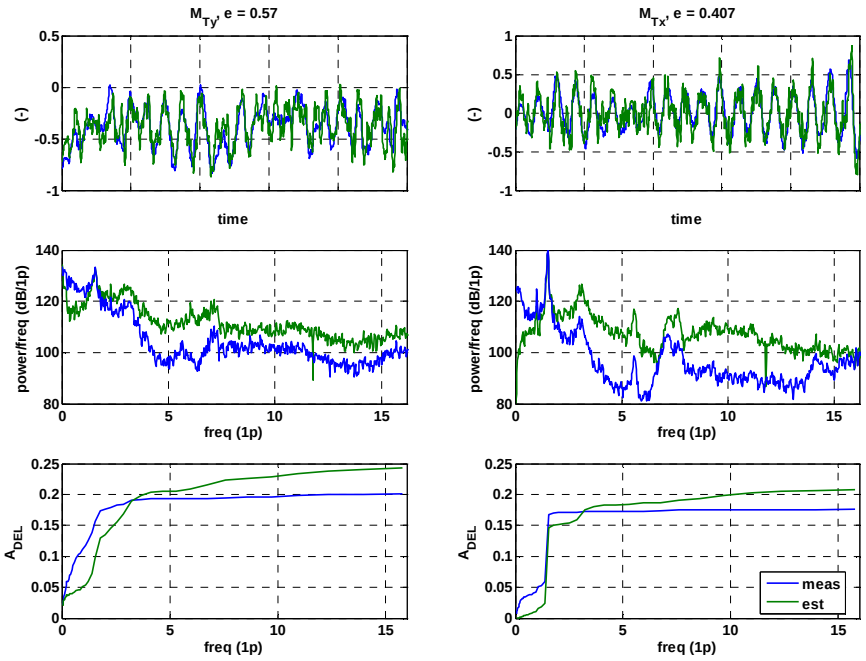

Figure 14: Longitudinal (left) and lateral (right) tower bending moment measurement (blue) and estimation with *external* wind speed estimation (green) at *18 m/s mean wind speed*. Top: time domain, center: frequency domain, bottom: frequency depending damage equivalent load. The normalized mean square error*) of the whole sequence is given in the title of the time domain plot.

4.2.2 Comparison of the wind speed estimation methods

In this subsection a closer look is taken at the wind speed estimation results using the internal and the external method. These are shown in Figure 15 in the time and in the frequency domain. A reliable reference measurement is not available because the anemometer is not very accurate. Hence, the methods can only be compared with each other.

In the low frequency range both methods lead to similar results, see, for example, the gust at 450 s in the sequence with 18 m/s mean wind speed. It is not unlikely that the estimations are more meaningful than the anemometer measurement – they “use” the whole wind turbine as a sensor for the average wind speed over the rotor plane.

A difference can be seen at frequencies above 1p. There, phenomena related to local wind speed at the blades are more pronounced in case of the internal estimation. For example, peaks at 3p-frequency due to the tower shadow and structural effects like the first tower mode at 1.5p at 18 m/s mean wind speed.

Of course, both methods can be enhanced. Regarding the external method the estimation of the current rotor power in Eq. (2.3) could involve a more sophisticated model including the drive train dynamics [3]. In this respect, the internal estimation has advantages because all structural dynamics are inherent.

The internal method is also more flexible and allows for the incorporation of rotor asymmetric wind speed effects. Preliminary tests with nx3p-Oscillators, asymmetric wind speed parts, and additional measurement signals[5] have been carried out. However, the estimation results

*) see Eq. (4.1)

[5] tower and blade bending moments

obtained with an observer design in line with section 3.2 were not satisfying. It is possible that a more sophisticated adjustment of weighting factors or other design approaches, see e.g. [17], might lead to improved results. On the other hand, from a practical point of view, the complexity of the design process has to be kept to a reasonable level.

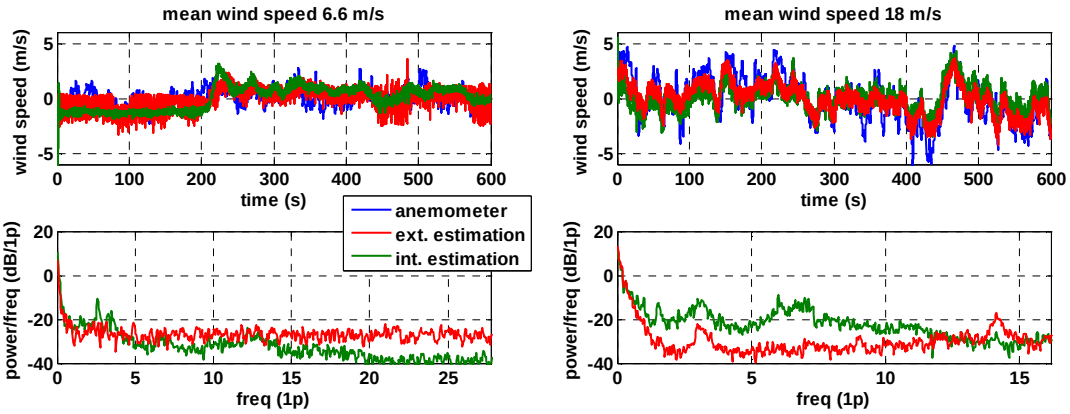

Figure 15: External (red) and internal (green) wind speed estimation and anemometer measurement (blue, only time domain). The upper and lower plots show the signals in the time and the frequency domain, respectively. Deflections from the mean values are shown in the time domain plot. Left: 6 m/s mean wind speed. Right: 18 m/s mean wind speed.

4.2.3 Estimation of blade bending moments

Although not the main focus of this work, this subsections presents the estimation results of the blade bending moments. The blades are part of the full model. Hence, an estimation of their bending moments is available using exactly the same sensor configuration as in the previous sections.

The collective flapwise and edgewise bending moments[6] are shown in Figure 16 in both time and frequency domain. These exemplary results have been obtained using the internal wind speed estimation for the measurement sequence at 18 m/s mean wind speed. Results at 6 m/s mean wind speed are comparable, but results – not shown here – with external wind speed estimation are much worse.

The estimation quality of the flapwise bending moments is fair. In the time domain the correlation is okay, what is also indicated by the normalized mean square error. In the frequency domain the correlation is quite good.

The estimation quality of the edwise bending moments is not bad in the frequency domain, too. But the time domain and the normalized mean square error are worse. This is mainly due to the dominant frequency peak at 1p that is caused by rotor asymmetries. These asymmetries are not included in the model and therefore very unlikely to be correctly reproduced.

While the collective blade bending moments are estimated okay this does not hold true for the asymmetric parts. Figure 17 shows the estimation results in the frequency domain. It can be seen that they are quite poor. Except for two peaks around 6p and 7.5p in the edgewise related plots. These peaks are the forward and backward wirling edgewise modes. However, the sensor basis (tower top accelerations, rotor speed and collective pitch) is not likely to capture much of asymmetric rotor related effects. Furthermore, none of these effects is explicitly integrated in the model. As already mentioned in the previous section, preliminary attempts to enhance the wind model both temporally and spatially have been carried out but did not lead to better estimation results.

[6] The collective part is the average over the three blades, i.e. $M_{fl,0} = \left(M_{fl,1} + M_{fl,2} + M_{fl,3}\right)/3$.

It is pointed out in section 3.1 that it might be sufficient for the estimation of blade related quantities to add the tower bending moments to the measurement signals. The advantage of this is that it is much easier to maintain sensors attached to the tower than to the blades.[7] This promising approach can be subject of further research.

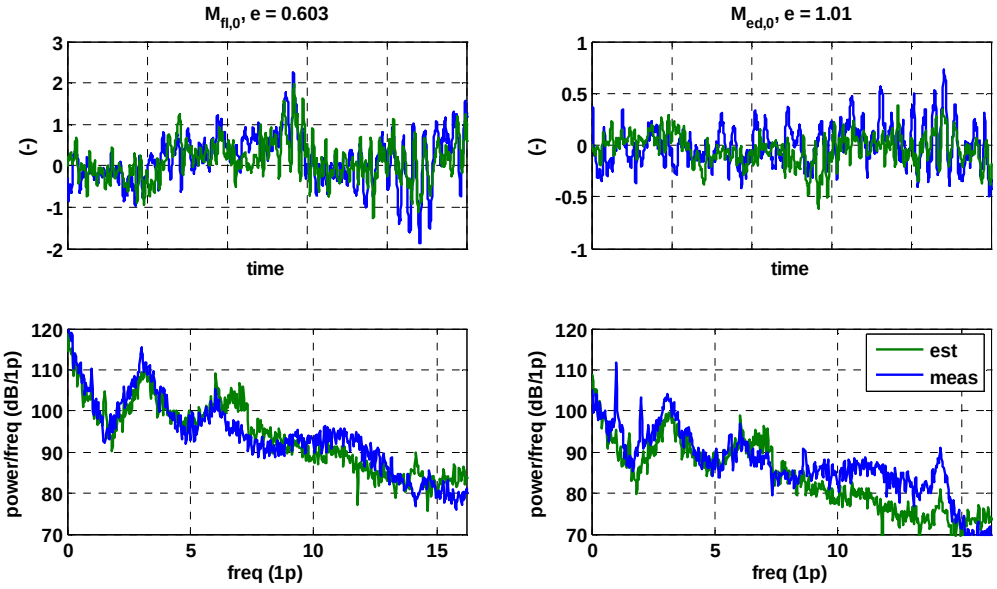

Figure 16: Measurement (blue) and estimation (green) of the collective blade bending moments using *internal* wind speed estimation at *18 m/s mean wind speed*. The upper and lower plots show the signals in the time and the frequency domain, respectively. Left: flapwise. Right: edgewise. The normalized mean square error*) of the whole sequence is given in the title of the time domain plot.

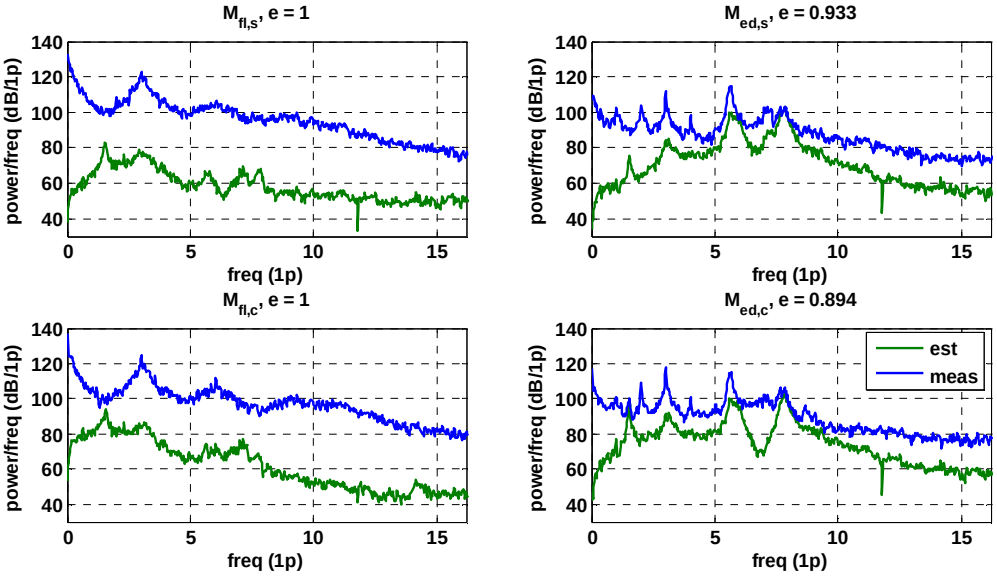

Figure 17: Frequency domain plots of measurement (blue) and estimation (green) of the asymmetric blade bending moments using *internal* wind speed estimation at *18 m/s mean wind speed*. The upper and lower plots show the sine and the cosine part, respectively. Left: flapwise. Right: edgewise. The normalized mean square error*) of the whole sequence is given in the title of the time domain plot.

[7] However, please note that prestress is very important for the fatigue loads of composite materials. That is, constant and slowly varying bending moments have to be estimated with high accurency.

*) see Eq. (4.1)

5 Conclusion

The online estimation of mechanical loads is useful in such different areas as load reducing control, structural health monitoring, and fault detection. This work provides a basic setting in order to do that using sensors readily available in today's large scale wind turbines. With measurements of the tower top acceleration in longitudinal and lateral direction, the rotor speed and the collective pitch angle it is possible to continuously estimate the tower bending moments. This has been verified for exemplarily measurement sequences in the region below and above rated wind speed using measurement data obtained from a field test on a commercially 5MW turbine.

Simple approaches involving linear models have been chosen because the intended applications are in the field of control. A state-space observer is used to estimate the current states of a linear time-invariant model of the wind turbine that is valid in the vicinity of a steady operating point. An easy to use procedure including only the choice of two scalar parameters is given for the observer design.

Since the model relies on the current wind speed and the measurement of the anemometer on top of the nacelle is too inaccurate, the wind speed has to be estimated as well. To this end, two different methods have been compared. The first one is the external method that uses the nonlinear rotor characteristics and measurements of the electrical power, the rotor speed and the collective pitch angle. The second one is the internal method, where a linear wind speed model excited by white noise is added to the wind turbine model and the observer estimates the states of both models at the same time.

In their specific design and implementation in this work both methods are based on the assumption that the wind field is sufficiently uniformly distributed over the rotor plane. Although they lead to comparable results concerning the estimation of the tower bending moments, the internal estimation method is preferable because it is not only more flexible with respect to the integration of asymmetric effects, but also superior regarding the estimation of the blade bending moments.

The estimation of the tower bending modes is quite good. Especially the loads regarding the first tower mode, which are the most significant parts in terms of fatigue load, are accurately estimated. Slowly varying loads below the first tower mode are not correctly captured by the approach. This might be due to neglecting rotor asymmetric effects. Using the internal wind speed estimation, promising results with estimating the collective blade bending moments have been obtained. Again, the absence of asymmetric effects in the model and the chosen sensor configuration limits the capacity of the approach to estimate rotor related quantities more accurately.

This issue can be subject of further investigations. As mentioned above, the internal wind speed estimation offers a wide flexibility including asymmetric effects. The flexibility can be utilized in conjunction with more sophisticatedly chosen weighting parameters in the observer design. Thus, the estimation of the blade bending moments can be improved.

Other possible developments include investigations that focus on time-varying operating points. In order to do this, a natural approach is gain-scheduling the model with the rotor speed and/or the pitch angle as scheduling variables. Another interesting possibility is an extended Kalman filter that inherently accounts for the nonlinear rotor characteristic.

6 References

[1] R. E. Kalman, R. S. Bucy. (1961). New Results in Linear Filtering and Prediction Theory. *Journal of Basic Engineering*, 83, pp. 95-108

[2] E. L. van der Hooft, T. G. van Engelen. (2003). Feed forward control of estimated wind speed. ECN-C-03-137

[3] T. Krüger: Regelungsverfahren für Windkraftanlagen zur Reduktion der mechanischen Belastung (in German), Dissertation, University of Kassel, 1998

[4] E. A. Bossanyi. (2000). Developments in Closed Loop Controller Design for Wind Turbines. *ASME Wind Energy Symp*., Reno, NV, US, pp. 64–74

[5] M. Hau. (2008). Promising load estimation methodologies for wind turbine components. Upwind Deliverable 5.2, http://www.upwind.eu/Shared%20Documents/WP5%20-%20Publications/D5.2_PromisingLoadEstimationMethodologies.pdf

[6] B. Jasniewicz, M. Geyler. (2011). Wind Turbine Modelling and Identification for Control Systems Applications. submitted to EWEA 2011

[7] Multibrid GmbH. (2010, June 8). M5000 Technical Data. Retrieved from http://www.multibrid.com/fileadmin/infomaterial/MB_Datenblatt_UK.pdf

[8] T. G. van Engelen. (2007). Control desing based on aero-hydro-sevo-elastic linear models from TURBU. ECN-M-07-054

[9] G. Bir. (2008). Multiblade Coordinate Transformation and Its Application to Wind Turbine Analysis. *ASME Wind Energy Symp*., Reno, NV, US

[10] E. A. Bossanyi. (2003). Individual blade pitch control for load reduction. *Wind Energy,* 6, pp. 119–128

[11] C. L. Botasso, A. Croce. (2009). Cascading Kalman Observers of Structural Flexible and Wind States for Wind Turbine Control, Dipartimento di Ingegneria Aerospaziale, Politecnico di Milano, DIA-SR 09-02

[12] K. Selvam, S. Kanev, J. W. van Wingerden, T. van Engelen and M. Verhaegen. (2009). Feedback-feedforward individual pitch control for wind turbine load reduction *International Journal of Robust and Nonlinear Control*, 19, pp. 72–91

[13] P. Caselitz, W. Kleinkauf, T. Krüger, J. Petschenka, M. Reichardt, K. Störzel. (1997). Reduction of Fatigue Loads on Wind Energy Converters by Advanced Control Methods. *Proceedings of the European Wind Energy Conference EWEC*, Dublin Castle, Ireland

[14] A. D. Wright, L. J. Fingersh, K. A. Stol. (2007). Designing and testing controls to mitigate tower dynamic loads in the controls advanced research turbine. *45th AIAA Aerospace Sciences Meeting and Exhibit, Wind Energy Symposium.*

[15] E. Bossanyi, A. Wright, P. Fleming. (2010). Controller field tests on the NREL CART2 turbine. Upwind Deliverable 5.6.1, http://www.upwind.eu/Shared%20Documents/WP5%20-%20Publications/D%205.6.1.pdf

[16] M. Geyler, B. Jasniewicz. (2010) . Parameter Estimation for Control Design Models Based on Operational Modal Analysis Techniques. DEWEK 2010

[17] A. Saberi, A. Stoorvogel, P. Sannuti. (2007). *Filtering Theory*. Birkhäuser.